ELSEVIER

Earth and Planetary Science Letters 185 (2001) 331–341

EPSL

www.elsevier.com/locate/epsl

Hydrogen isotope analysis of rehydrated silicic lavas: implications for eruption mechanisms

P.J. DeGroat-Nelson, B.I. Cameron *, J.H. Fink, J.R. Holloway

Department of Geological Sciences, Box 871404, Arizona State University, Tempe, AZ 85287-1404, USA

Received 3 April 2000; received in revised form 8 December 2000; accepted 11 December 2000

Abstract

Bulk and step-heating hydrogen isotope measurements of glassy and vesicular samples from three young rhyolite lavas demonstrate for the first time that magmatic H_2O can be distinguished from meteoric H_2O added during rehydration. Step-heat extractions of gases obtained at five temperatures show that most meteoric H_2O is released at around 400°C, while magmatic H_2O comes off during the fusion step at 1100–1200°C. Magmatic H_2O contents from vertically-arrayed lava samples show a downward increase consistent with the equilibrium pressure-dependence of H_2O solubility. These gradients imply that volatile concentrations high enough to generate pyroclastic flows during front collapse may be found in the upper portions of silicic domes produced by relatively high eruption rates.

Keywords: D/H; meteoric water; obsidian; hydration of glass; domes; volcanic risk

1. Introduction

The hazard potential of any active volcano is strongly influenced by the way volatiles are released from its magma prior to, during, or after an eruption. H_2O and hydrogen isotope measurements of glassy eruption products from various volcanic centers have helped clarify how degassing occurs in silicic systems [1–5]. The general picture that has emerged is that high initial volatile contents (5–7 wt%) in the magma chamber are mostly lost to the atmosphere and into the walls of the conduit by 'open-system' degassing during ascent and eruption [6,7]. The amount of residual volatiles (0.1–1.0 wt%) determines whether erupting magma comes out explosively or effusively. Low eruption rates allow more of the initial H_2O to escape during rise and favor the emplacement of lava flows and domes, while high rates lead to more violent eruptions of gas-rich products [8]. Transitions in eruptive behavior should relate to slight gradients in magmatic volatile contents as well as to variations in eruption rate. However, no previous studies have been able to document these subtle compositional differences nor show how they relate to explosivity.

Although lava domes are made up of magma that has lost most of its magmatic H_2O, some are still capable of generating deadly pyroclastic flows when their flow fronts collapse and expose their

* Corresponding author. Tel.: +1-480-965-9852; Fax: +1-480-965-8102; E-mail: barry.cameron@asu.edu

0012-821X/01/$ – see front matter
PII: S0012-821X(00)00379-4

hot, pressurized interiors. Such events have killed dozens of people in the 1990s in Japan, Indonesia, and on the Caribbean island of Montserrat. The energy of this sort of 'endogenous' explosive activity is proportional to the residual H_2O content of the lava [9]. Thus, knowing the distribution of H_2O within lava domes is crucial for evaluating their hazards. However, the H_2O contents of the upper portions of lavas may also be affected by rehydration [10–12], a temperature-, time-, and porosity-dependent process governed by the diffusion of molecular H_2O into the glass structure [13–16]. This addition of meteoric H_2O, particularly for vesicular samples that have relatively large surface areas, seriously complicates attempts to relate juvenile volatile contents to magma chamber or eruptive processes.

Because degassed magmatic and meteoric H_2O at a single flow commonly have significantly different stable isotope signatures, it should theoretically be possible to identify rehydration in a glassy or pumiceous sample using bulk isotopic methods. Moreover, by step-heating crushed samples up to temperatures of 400°C and stripping off the non-magmatic H_2O [17,18], we have developed the ability to 'see through' meteoric alteration and identify the primary magmatic H_2O content of rehydrated glassy and vesicular lavas. This approach greatly expands the opportunities for interpreting the eruptive histories and hazard potential of silicic magmas.

2. Background

To assess the impact of rehydration on silicic lavas, we selected three well-studied Holocene age rhyolite flows from the western United States that each exhibits a variety of vesicular and glassy surface textures: Little Glass Mountain and Glass Mountain from Medicine Lake Volcano in northern California, and Obsidian Dome adjacent to Long Valley Caldera in eastern California. Most samples were collected from 3–8 m tall spines that project above the flow surface and exhibit a textural gradation from dense and glassy at the base to highly vesicular at the top. Others were taken from transects that crossed similar textural gradients along diapirs exposed at the flow surface. To facilitate comparison, our samples were classified, both by eye and through helium pycnometry, into one of three textural types: (1) obsidian (OBS; black with less than 10% vesicles); (2) mid-texture (MID; banded dark gray and black, with 10–25% vesicles); and (3) finely vesicular pumice (FVP; light gray with 25–40% vesicles). In practice, only OBS and FVP samples could be consistently distinguished in the field; MID samples were selected based as much on their position in a spine or on the flow surface as on their appearance.

3. Hydrogen isotope measurements

We carried out two sets of hydrogen isotope measurements. First, a large suite of glassy and vesicular rocks from the surface of each flow was examined using whole-rock fusion analyses, to identify and confirm rehydration in the more vesicular samples. A subset was then step-heated, which allowed us to discern specific 'types' and amounts of H_2O within each sample. Samples were initially prepared at Arizona State University (ASU) by breaking a portion of each into chips between 1 and 2 mm in longest dimension. Chips were then hand-picked under a plain-light binocular microscope to eliminate pieces that appeared to have organic contamination, highly oxidized areas, or obvious mineral inclusions. The remaining fragments were then crushed to an average diameter of 0.1 mm and shipped to the Stable Isotope Laboratory at Southern Methodist University (SMU). At SMU, samples were again inspected for organic contamination or unusual appearance. Approximately 100 mg of suitable material was then introduced into a molybdenum crucible and heated at 40°C overnight under vacuum to remove most H_2O adsorbed on the surface. For each analysis, H_2 and H_2O (reacted with uranium to produce H_2) were collected to yield (D/H) values that were then converted to δD relative to SMOW. Hydrous fluid was measured manometrically and is reported as wt% H_2O, although the actual volatile sample may contain a mixture of molecular H_2O, ionic OH^- and H_2

gas. The 1σ error for all analyses is ± 0.005 wt% for H_2O and ± 1–4‰ for δD (K. Ferguson, SMU, personal communication, 1997).

For standard fusion analyses, samples were heated until melted at between 1100 and 1200°C. They were held at this fusion temperature until a sharp decrease in volatile loss rate was noted (usually after 30–45 min) and the remaining volatile loss was within the range of error (i.e. close to zero). The duration of heating was limited to reduce the possibility of contamination from breakdown of the molybdenum crucible. Our study includes 90 samples analyzed in this way: 44 from Little Glass Mountain, 31 from Glass Mountain, and 15 from Obsidian Dome. Table 1 summarizes the results of our bulk rock hydrogen isotope analyses.

During step-heating analyses, released volatiles were collected separately for temperatures of approximately 100, 200, 400, and 600°C as well as a fusion step at 1100–1200°C. Each temperature step below fusion was maintained for approximately 2 h, and derived volatiles were collected and analyzed as described above. Step-heating was performed in this manner for a minimum of three samples (one each of FVP, MID, and OBS) from each of the three flows. For Little Glass Mountain, a set of FVP, MID, and OBS samples from a diapir and spine were analyzed, and one of the FVP samples from the spine (LG94-02C) was

Table 1
Bulk hydrogen isotope data and H_2O contents for variably-textured, glassy lavas from three domes in California

Sample	Texture	H_2O (wt%)	δD (‰)	Sample	Texture	H_2O (wt%)	δD (‰)	Sample	Texture	H_2O (wt%)	δD (‰)
Glass Mountain				*Little Glass Mountain*				*Little Glass Mountain (con't)*			
GM94-10	OBS	0.14	−152.2	LG94-01A	OBS	0.21	−139.0	LGS95-02D	FVP	0.49	−107.3
GM94-11	OBS	0.13	−146.5	LG94-01B	OBS	0.12	−153.3	LGS95-03A	MID	0.33	−93.9
GM95-02	OBS	0.13	−120.0	LG94-01C	FVP	0.29	−127.2	LGS95-03B	MID	0.32	−95.8
GM95-03	MID	0.24	−111.0	LG94-02A	OBS	0.21	−152.0	LGS95-03C	MID	0.35	−96.5
GM95-04A	FVP	0.39	−97.1	LG94-02B	OBS	0.29	−127.9	LGS95-03D	MID	0.33	−102.2
GM95-04B	FVP	0.31	−104.7	LG94-02C	FVP	0.62	−93.1	LG97-01	OBS	0.11	−127.9
GM95-05A	FVP	0.46	−90.8	LG94-03	OBS	0.18	−136.5	LG97-02	MID	0.24	−126.9
GM95-05B	FVP	0.42	−90.1	LG94-04	OBS	0.12	−161.4	LG97-03	MID	0.25	−107.3
GM95-06	OBS	0.14	−117.1	LG94-05A	OBS	0.19	−123.4	LG97-04A	MID	0.27	−95.2
GM95-07	OBS	0.10	−126.3	LG94-05B	MID	0.18	−135.1	LG97-04B	FVP	0.66	−86.8
GM95-08	MID	0.10	−116.5	LG94-05C	MID	0.14	−113.8	LG97-05	OBS	0.10	−140.0
GM95-09	MID	0.24	−111.6	LG94-05D	MID	0.50	−87.3	LG97-J01	OBS	0.10	−143.5
GM95-10A	FVP	0.74	−87.2	LG95-01	OBS	0.18	−115.7	LG97-J02	MID	0.26	−93.5
GM95-10B	FVP	0.58	−77.6	LG95-02	OBS	0.12	−128.6				
GM95-10C	FVP	0.48	−79.3	LG95-03B	MID	0.28	−102.0	*Obsidian Dome drill core*			
GM95-11	OBS	0.12	−142.9	LG95-04	FVP	0.84	−90.4	OBC-1	FVP	0.44	−110.3
GM95-12	MID	0.13	−121.8	LG95-05	OBS	0.15	−131.7	OBC-2	MID	0.27	−131.1
GM95-13	FVP	0.53	−90.6	LG95-06A	MID	0.34	−105.6	OBC-3	FVP	0.37	−134.4
GM95-14A	FVP	0.43	−81.6	LG95-06B	MID	0.33	−99.2	*Obsidian Dome flow front*			
GM95-14B	FVP	0.53	−85.2	LG95-07	FVP	0.71	−88.5	OD95-01	OBS	0.16	−120.8
GM95-14C	FVP	0.42	−99.4	LG95-08A	FVP	0.78	−77.5	OD95-02	MID	0.32	−107.0
GM95-15	OBS	0.11	−138.1	LG95-08B	FVP	0.66	−90.2	OD95-05	FVP	0.96	−76.9
GM95-16	MID	0.23	−104.3	LG95-09A	OBS	0.11	−126.2	OD95-09	OBS	0.16	−139.3
GM95-17	FVP	0.52	−88.6	LG95-09B	OBS	0.15	−139.0	OD95-10	MID	0.29	−111.1
GM95-18A	FVP	0.43	−81.7	LGS95-01A	OBS	0.08	−136.9	OD95-11	FVP	0.55	−90.8
GM95-18B	FVP	0.46	−76.6	LGS95-01B	MID	0.24	−108.5	OD95-12	OBS	0.16	−117.7
GM95-18C	FVP	0.50	−78.0	LGS95-01C	FVP	0.35	−91.3	OD95-13	OBS	0.13	−114.6
GM97-01	OBS	0.06	−139.1	LGS95-01D	FVP	0.73	−92.6	OD95-14	MID	0.16	−108.9
GM97-02	OBS	0.07	−139.4	LGS95-02A	OBS	0.16	−131.8	OD95-15	FVP	0.36	−108.5
GM97-03A	OBS	0.10	−131.9	LGS95-02B	FVP	0.34	−93.7	OD95-16A	FVP	0.80	−105.1
GM97-03B	OBS	0.10	−143.5	LGS95-02C	FVP	0.43	−88.3	OD95-16B	FVP	0.75	−100.3

Table 2
Step-heating hydrogen isotope and H_2O content data for selected glassy lavas from three lava domes in California

Sample	Texture	Dist. (m)	$H_2O^{100°C}$ (wt%)	$\delta D^{100°C}$ (‰)	$H_2O^{200°C}$ (wt%)	$\delta D^{200°C}$ (‰)	$H_2O^{400°C}$ (wt%)	$\delta D^{400°C}$ (‰)	$H_2O^{600°C}$ (wt%)	$\delta D^{600°C}$ (‰)	H_2O^{Fusion} (wt%)	δD^{Fusion} (‰)	$H_2O^{cumul.}$ (wt%)	$\delta D^{cumul.}$ (‰)
Glass Mountain														
GM95-17	FVP	−1.0	0.008	−79.0	0.091	−78.9	0.28	−75.5	0.074	−88.1	0.064	−116.7	0.51	−83.1
GM95-04A	FVP	−3.0	0.004	−82.4	0.048	−83.1	0.17	−77.6	0.071	−106.1	0.073	−142.3	0.37	−96.5
GM95-16	MID	−2.0	0.002	−91.6	0.018	−65.7	0.073	−67.9	0.040	−77.3	0.091	−118.9	0.22	−90.3
GM95-03	MID	−5.0	0.002	−96.4	0.023	−91.1	0.10	−91.2	0.046	−105.0	0.079	−134.8	0.25	−107.6
GM95-15	OBS	−3.0	0.001	−109.7	0.002	−72.9	0.003	−111.7	0.003	−121.9	0.092	−126.1	0.10	−124.2
Little Glass Mountain														
LG94-02C	FVP	−1.0	0.009	−80.8	0.085	−77.0	0.29	−70.3	0.066	−83.5	0.070	−121.3	0.53	−80.0
LG94-02C[a]	FVP	−1.0	0.007	−62.5	0.13	−74.3	0.30	−65.8	0.061	−60.3	0.060	−118.9	0.56	−72.9
LG95-08A	FVP	−1.0	0.005	−86.4	0.12	−67.7	0.42	−57.4	0.12	−62.1	0.08	−105.8	0.74	−65.1
LG94-05D	MID	−0.5	0.008	−54.1	0.12	−64.5	0.27	−57.2	0.053	−54.3	0.059	−115.4	0.51	−65.2
LG95-06A	MID	−4.0	0.002	−114.0	0.042	−81.5	0.16	−80.6	0.059	−93.0	0.10	−119.4	0.36	−93.4
LG94-02A	OBS	−3.0	0.001	−43.6	0.008	−57.0	0.028	−61.9	0.009	−106.6	0.084	−121.1	0.13	−102.8
LG95-05	OBS	−6.0	0.00	n.d.	0.003	−102.4	0.004	−89.8	0.005	−106.3	0.12	−117.3	0.13	−115.6
Obsidian Dome														
OD95-16A	FVP	−2.0	0.008	−81.4	0.23	−81.2	0.44	−80.7	0.076	−100.3	0.033	−117.1	0.79	−84.3
OBC-3	FVP	−8.9	0.009	−51.1	0.097	−81.8	0.13	−103.9	0.074	−114.2	0.067	−138.5	0.38	−104.2
OD95-15	MID	−4.0	0.007	−105.9	0.059	−99.8	0.16	−96.8	0.052	−117.9	0.033	−139.6	0.31	−105.6
OD95-13	OBS	−8.0	0.00	n.d.	0.017	−92.1	0.026	−85.4	0.024	−108.3	0.072	−121.5	0.14	−108.9

[a]Duplicate analysis; n.d. = not determined.

Table 3
δD values for surface water samples from Medicine Lake Volcano, Long Valley Caldera and Hot Creek Basin, California

Location	Sample location	δD meteoric water (‰)	Estimated error	Reference
Obsidian Dome	Deadman Creek	−124.4		[19]
	Hartley Springs	−126.3		[19]
	Crystal Spring	−98.5	±5–12	[19]
Medicine Lake	Schonchin Spring	−97.7	±5–12	[20]
	Lost Spring	−97.8	±5–12	[20]
	Eastman Spring	−102.1	±5–12	[20]
	Range	−92 to −98		[1]
Hot Creek Basin	Large-volume springs	−95 to −106		[21]
	Evaporated waters	−63 to −92		[21]

analyzed twice to check for reproducibility. There is excellent agreement between the amount of H_2O released at each temperature step for the duplicate sample, although the δD values exhibit slight differences. Variations in the release of H_2O can easily result from diffusion out of different shaped and sized glass chips. The overall agreement between the bulk rock measurement and the cumulative H_2O and δD value calculated for each step-heat analysis inspires confidence in the step-heat technique. Table 2 presents the results of our step-heating hydrogen isotope analyses.

The average hydrogen isotope composition of present-day meteoric H_2O was estimated for regions close to each dome (Table 3). It is not always clear how waters taken from nearby streams, springs, or puddles relate to the precipitation affecting the isotopic signature of a lava flow, but these were generally the only available independent measurements. These meteoric values are generally higher (i.e. more enriched) in δD (−90 to −130‰) than those reported in the literature for non-vesicular obsidian (−120 to −160‰) for the areas under consideration [1,2,4].

4. Evidence for rehydration

The addition of meteoric H_2O to a glassy volcanic obsidian or pumice causes a hydration layer to form along every exposed surface. As molecular H_2O diffuses into the drier interior, a waxy-looking 'hydration rind' appears at the sample's surface [15,16]. The temperature-dependence of this process for volcanic glasses can be expressed as follows:

$$\ln D = -C - E/(RT)$$

where D = diffusivity (m^2/s), $C = 15.22$ = constant which takes into account glass composition (m^2/s), $E = 8.67 \times 10^5$ J/mol = activation energy, $R = 8.317$ J/K-mol = universal gas constant, and T = temperature (K). The amount of rehydration a glassy lava sample experiences depends on its surface area. Thus pumice with an abundance of interconnected vesicles can absorb more H_2O

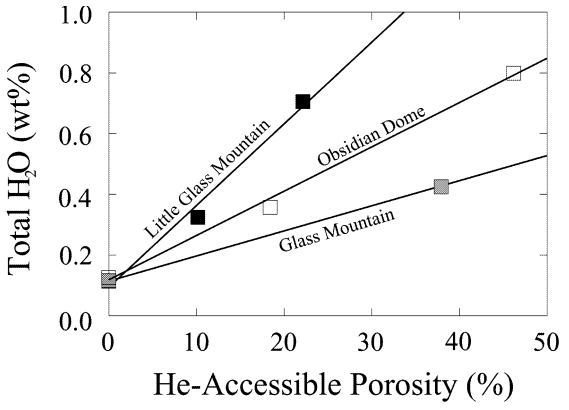

Fig. 1. H_2O concentration versus helium-accessible porosity (a measure of connected vesicle porosity) determined by helium pycnometry, for the three flows in this study. Separate regression lines are drawn for each flow. Error bars on the H_2O measurements would be smaller than the symbols.

than bubble-free obsidian. We confirmed this relationship by plotting the connected porosity of rehydrated glassy and vesicular samples from each of the flows in our study against their total H_2O contents (Fig. 1). In every case, H_2O is proportional to porosity; OBS has consistently lower H_2O contents than adjacent MID or FVP samples. Differences in slope for the data sets may reflect variations in lava chemistry, position of the sample in the volcanic spine or transect, age, or local precipitation rates or amounts.

For each lava flow, whole-rock fusion analyses revealed a gradient from low (i.e. depleted) δD for obsidian up to a higher (i.e. enriched) value for the most pumiceous samples (Fig. 2). We assume that this trend reflects the admixture of increasing amounts of meteoric H_2O in the more vesicular rocks. Simple proportional mixing models that combine the most depleted and enriched δD values for each location can account for most of the data. These curves suggest that the relevant meteoric δD values are $-75‰$ for Little Glass Mountain, $-70‰$ for Glass Mountain, and $-100‰$ for Obsidian Dome. These values are more enriched than those measured in meteoric H_2O samples near the lava flows today (Table 3).

Step-heat isotope results for Glass Mountain, Little Glass Mountain, and Obsidian Dome are presented as fractional H_2O content versus temperature in Fig. 3 and δD versus cumulative wt% H_2O in Fig. 4. Analytical problems associated with the extremely small amount of H_2O liberated during the 100°C step produced wide variations in the δD values and we are hesitant to adopt this low temperature step as a meteoric signature. Instead, we prefer to consider the pronounced spike of deuterium-enriched H_2O lost during the 200 and 400°C steps from the vesicular samples (Fig. 3) more representative of the meteoric component. The meteoric H_2O value determined by the step-heat analysis ranges in δD from $-59.4‰$ to $-98.3‰$. Although this range might seem large and only overlaps the assumed local meteoric H_2O values at the most depleted end, it does closely match the range for evaporated surface waters in the Hot Creek Basin region of northeastern California (Table 3). Evaporation of surface waters represents a plausible explanation for

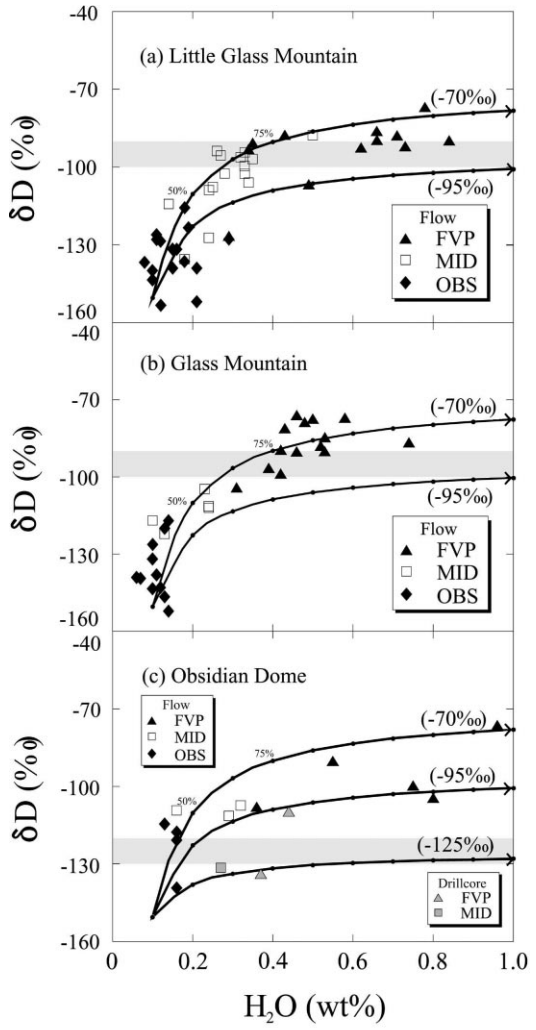

Fig. 2. δD versus H_2O for whole-rock analyses of samples from (a) Little Glass Mountain, (b) Glass Mountain, and (c) Obsidian Dome. Curves were calculated from simple mixing of assumed degassed magmatic end member with a δD of $-150‰$ and a H_2O content of 0.1 wt% and a variety of possible meteoric signatures (in parentheses). The percentage of meteoric H_2O is shown next to select tick marks on the upper mixing curve in each panel. The lower curve in each panel corresponds to mixing with meteoric end members comparable to modern values ($\pm 5‰$, indicated by shading). Note that for each flow, the curves that best fit the data are for meteoric signatures higher than modern values. Error bars on H_2O measurements would be smaller than the size of the symbols, whereas error bars for the δD values would be close to the symbol size.

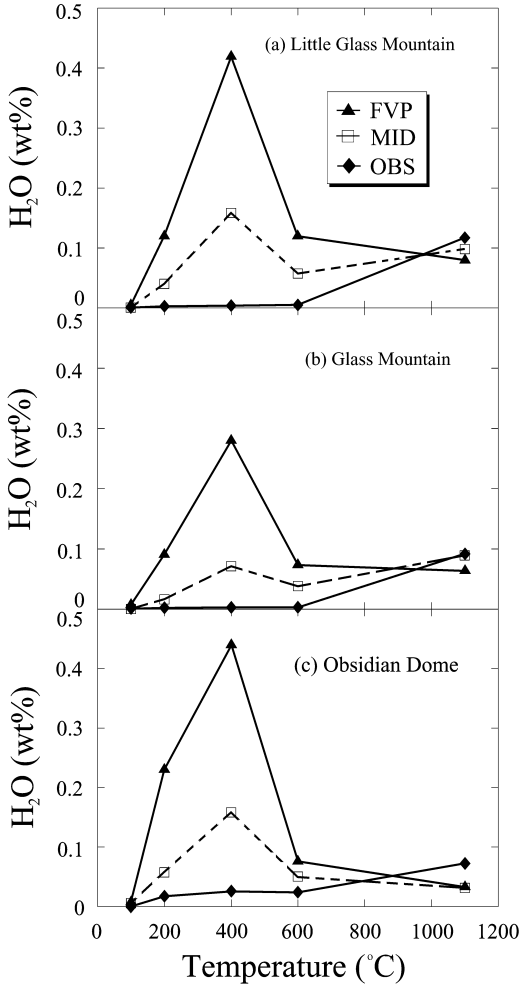

Fig. 3. H_2O versus temperature for step-heat analyses of a set of three textures from (a) Little Glass Mountain, (b) Glass Mountain, and (c) Obsidian Dome. Note that in all cases, the FVP and MID samples give off most of their H_2O at the 400°C temperature step, and that the OBS samples release the most H_2O at the highest temperature step.

the enriched composition of the meteoric end member in simple mixes with degassed magmatic H_2O based on the bulk rock hydrogen isotope measurements (Fig. 2).

The H_2O lost from all three textures during the high temperature fusion step is most likely of a degassed magmatic origin. H_2O from step 4 (600°C) is probably a mixture of both types. If we assume that the intermediate δD values measured in step 4 are linear combinations of meteoric and degassed magmatic end members, then the amounts of the two types of H_2O extracted at this temperature should scale as the relative proportions of the isotopic signatures. The amount of degassed magmatic H_2O for each texture at each flow was calculated in this manner (Table 4). For example, steps 2 and 3 for an analysis of FVP sample OD95-16A from Obsidian Dome yielded

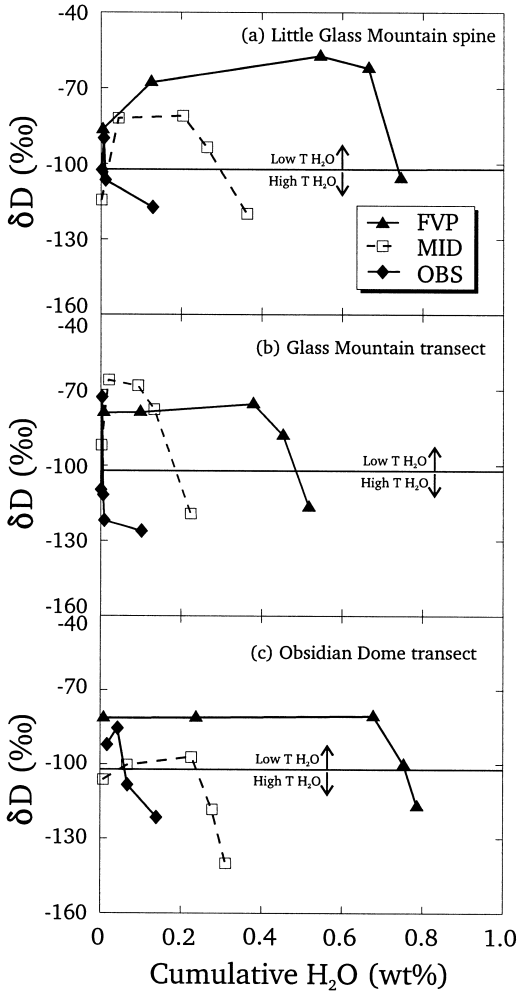

Fig. 4. δD versus cumulative H_2O for step-heat analyses of a set of three textures from (a) Little Glass Mountain, (b) Glass Mountain, and (c) Obsidian Dome. Approximate delineation between high and low temperature H_2O species is shown by horizontal line. OBS samples from Little Glass Mountain and Glass Mountain show variable δD values for the low temperature steps because too little H_2O was released to accurately measure δD.

δD values of −81.2 and −80.7‰ (average = −81.0‰), step 4 yielded −100.3‰, and step 5 (fusion) for an adjacent OBS sample yielded −121.5‰. If we assume that the meteoric value is −81.0‰ and the magmatic value is −121.5‰, then step 4's value of −100.3‰ can be considered a mixture of 52% meteoric and 48% magmatic. Apportioning the 0.080 wt% total H_2O released during step 4 in the same way, we find meteoric and magmatic contributions of 0.042 and 0.038 wt%, respectively. The 0.038 wt% can then be added to the 0.030 wt% derived at the highest temperature step to give a total magmatic fraction of 0.068 wt% for this FVP sample.

Using the above assumptions, the calculated magmatic H_2O content in the step-heated samples from the three silicic flows was plotted in Fig. 5 as a function of either depth beneath the upper flow surface or lateral distance along a transect (which is equivalent to depth; Fig. 6). The magmatic H_2O content in the Little Glass Mountain, Glass Mountain, and Obsidian Dome drill core samples increases toward the flow interior (or center of the transect) at a rate of approximately 0.010 wt% per m (Fig. 5, dashed line). This rate closely matches the gradient predicted for near 1 ATM conditions by the pressure-dependence of H_2O solubility in rhyolite glass at 900°C (Fig. 5, solid curve), which is nearly linear at these low pressures [23,24]. The calculated magmatic H_2O contents all lie slightly to the left of the saturation curve. This offset may reflect errors in the simple calculation of the magmatic H_2O content or that a value of 0.234 bars/m overestimates the density of the vesiculated obsidian. These near 1 ATM estimates assume equilibrium saturation values, and that solubility varies only with pressure. However, prior to collection, the samples were all exposed to the atmosphere, either along the transects or on the vertical faces of the uplifted spines. The measured gradients thus imply that equilibration of H_2O took place throughout the upper portion of the flow prior to the fracturing and disruption that pushed up the spines or otherwise exposed the interior lava to the atmosphere (Fig. 6). Because some Obsidian Dome samples were taken from the flow front, they do not show a similar pressure-dependent gradient in H_2O.

Table 4
Calculated magmatic H_2O contents based on step-heat analyses

Sample	Texture	Dist. (m)	δD^{a}_{Met} (‰)	δD^{b}_{Mag} (‰)	Prop. Met.	Prop. Mag.	Met. H_2O (wt%)	Mag. H_2O (wt%)
Glass Mountain								
GM95-17	FVP	−1.0	−78.9	−126.1	0.805	0.195	0.436	0.074
GM95-04A	FVP	−3.0	−80.4	−126.1	0.438	0.562	0.253	0.113
GM95-16	MID	−2.0	−66.8	−126.1	0.823	0.177	0.123	0.097
GM95-03	MID	−5.0	−91.2	−126.1	0.605	0.395	0.153	0.097
GM95-15	OBS	−3.0	−92.3	−126.1	0.124	0.876	0.0064	0.093
Little Glass Mountain								
LG94-02C	FVP	−1.0	−73.6	−121.1	0.792	0.208	0.445	0.084
LG94-02C	FVP	−1.0	−70.0	−121.1	1.000	0.000	0.500	0.060
LG95-08A	FVP	−1.0	−62.6	−121.1	1.000	0.000	0.660	0.080
LG94-05D	MID	−0.5	−60.8	−121.1	1.000	0.000	0.450	0.060
LG95-06A	MID	−4.0	−81.0	−121.1	0.701	0.299	0.245	0.118
LG94-02A	OBS	−3.0	−59.4	−121.1	0.235	0.765	0.042	0.088
LG95-05	OBS	−6.0	−96.1	−121.1	0.408	0.592	0.004	0.126
Obsidian Dome								
OD95-16A	FVP	−2.0	−81.0	−121.5	0.465	0.535	0.722	0.068
OBC-3	FVP	−8.9	−92.8	−121.5	0.254	0.746	0.252	0.122
OD95-15	MID	−4.0	−98.3	−121.5	0.155	0.845	0.238	0.072
OD95-13	OBS	−8.0	−88.8	−121.5	0.404	0.596	0.058	0.082

[a]The δD value of meteoric H_2O is taken as the mean of the 200°C and 400°C step.
[b]The δD value of the magmatic H_2O is taken as the δD of the fusion step for a massive obsidian sample from that dome.

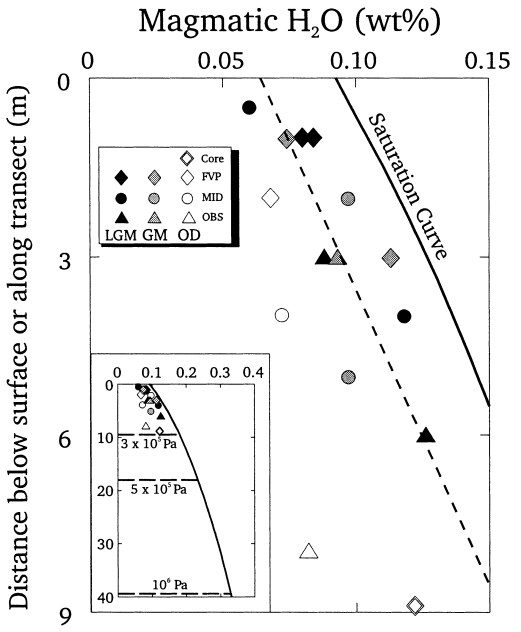

Fig. 5. Depth from top of spine or distance from end of transect versus magmatic H_2O content for variably textured step-heated samples from Little Glass Mountain (LGM), Glass Mountain (GM), and Obsidian Dome (OD). Solid line shows the pressure-dependence of H_2O solubility for rhyolite at 900°C and low pressures. The saturation pressures for the H_2O solubility curve were determined using an Excel-based software program called VolatileCalc provided by Jake Lowenstern of the USGS. Pressures were converted to depths assuming an atmospheric pressure of 0.78 bars for an approximate elevation of 2000 m and a density for obsidian of 0.234 bars/m [22]. A regression line through the Glass Mountain, Little Glass Mountain, and Obsidian Dome drill core step-heat samples lies parallel to the experimental H_2O solubility curve. The saturation curve effectively serves as an upper limit for the calculated magmatic H_2O contents. Inset: The volatile pressure exceeds the maximum surface crust strength of 10^6 Pa at a depth of approximately 39 m. When more realistic surface crust strengths of 3 and 5×10^5 Pa are considered, volatile pressure excesses occur at depths of about 9.5 and 18 m, respectively.

5. Hazard implications

From a hazards standpoint, the main reason to study lava domes is to discover real-time clues that active domes are more or less likely to explode if their fronts collapse suddenly. If we assume that such violent behavior occurs when volatile pressure exceeds the strength of the lava [9], then we need ways to estimate these two variables.

In recent morphologic studies based on laboratory simulations [25,26], domes were classified into several types controlled by eruption rate and strength of their surface crust. Domes extruded at the lowest rates and made of lavas with the strongest carapace tend to be steep-sided, covered with tall spines, cut by fractures, and show relatively little variation in vesicularity. Such textural homogeneity implies that volatiles are evenly distributed. In contrast, the highest eruption rates and lowest surface crust strengths yield flows that are less steep-sided, less tall, less fractured, and more texturally diverse. This type also may contain explosion craters, 5–15 m deep, formed when internal volatile pressure exceeds the strength of the carapace [7]. The three flows in the current study are all of the latter type, suggesting that they had relatively high effusion rates, more variable volatile contents and weak crusts. Fink and Griffiths [25] calculated maximum strengths of approximately 10^6 Pa for this type of flow. Fractures would further reduce the strength of the weak surface crusts of the three flows. The strength of the surface crust for the Mount St. Helens dacite dome was estimated between 10^5 and 10^7 Pa [9].

The measured gradients in magmatic H_2O re-

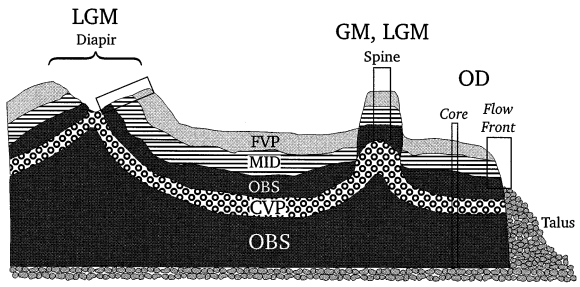

Fig. 6. Schematic drawing showing the textural stratigraphy in the upper portion of rhyolitic obsidian flows (after [7]). Rectangles show sample collection sites. Profiles through spines were sampled at Glass Mountain (GM), whereas samples were collected from both transects along diapirs and profiles through spines at Little Glass Mountain (LGM). Spines and diapirs both result from buoyancy of underlying coarsely vesicular pumice (CVP) zone. At Obsidian Dome (OD), samples were taken both from a profile of the steep flow front and drill core.

ported here for Little Glass Mountain and Glass Mountain, if extrapolated inward, imply that volatile pressures would exceed the maximum surface crust strength of 10^6 Pa at $\sim$39 m below the surface. Volatile pressures in the interior of the silicic flow surpass more realistic estimates of surface crust strengths (e.g. 3 and 5×10^5 Pa) at depths of 9.5 and 18 m, respectively (Fig. 5, inset). These more closely correspond to the depth of explosion craters found on the surfaces of both flows. It is also the approximate depth of a volatile-enriched layer found in two cores drilled through Obsidian Dome [27]. These extrapolated H_2O contents for the interior of the flows are significantly higher than the 1 ATM saturation values for rhyolite, which indicates that the lava did not fully equilibrate upon emerging from the vent, contrary to the widely cited 'permeable foam' model [6].

During its 6-yr growth, the well-documented Mount St. Helens dacite dome had only one notable explosive event, a lateral blast that preceded emplacement of the March 1982 lobe [28]. This lobe had a relatively high eruption rate and contained anomalously dark lava, which presumably had higher H_2O concentrations. Longitudinal profiles of H_2O contents in several other lobes of this dome showed increases toward the vent [5,7], making it less likely that the conditions necessary for explosions (thin crusts and high volatile contents near the flow front) would occur.

The current results suggest that rhyolitic lavas erupted at relatively high extrusion rates may contain concentrations of volatiles capable of undergoing major explosive decompression events. However, explosion pits and craters on the flows' upper surfaces are the only direct evidence of these energetic conditions, since pyroclastic flows associated with rhyolite dome emplacement have never been witnessed. In contrast, domes whose magmas have lower bulk silica contents, such as the andesites at Soufriere Hills, Montserrat, and Merapi in Indonesia, frequently produce pyroclastic phenomena from their flow fronts. These magmas have significantly higher concentrations of microlites [29,30] and phenocrysts, all of which may lead to higher yield strengths capable of retaining greater volatile pressures without spontaneously exploding. When the over-pressurized interior magma is exposed to the atmosphere during flow-front collapse, it is more likely to generate explosions than its more silicic, glassy counterparts. Quantifying the endogenic explosive potential for these less silicic domes will require comparable measurements of magmatic volatile gradients coupled with better field-based estimates of eruption rate and laboratory measurements of yield strength.

Acknowledgements

Thanks to L. Paul Knauth and C.R. Manley for helpful discussions, and S. Sparks and N. Dunbar for constructive reviews that led to substantial improvements in the manuscript. Research supported by NSF grants OCE 93-16831 and EAR 96-14330, and NASA grant NAGW 529.*[AH]*

References

[1] B.E. Taylor, J.C. Eichelberger, H.R. Westrich, Hydrogen isotopic evidence of rhyolitic degassing during shallow intrusion and eruption, Nature 306 (1983) 541–545.
[2] S. Newman, S. Epstein, E. Stolper, Water, carbon dioxide, and hydrogen isotopes in glasses from the ca. 1340 A.D. eruption of the Mono Craters, California: Constraints on degassing phenomena and initial volatile content, J. Volcanol. Geotherm. Res. 35 (1988) 75–96.
[3] B.E. Taylor, Magmatic volatiles: Isotopic variation of C, H, and S, in: J.W. Valley, H.P. Taylor, Jr., J.R. O'Neil (Eds.), Stable Isotopes in High Temperature and Geological Processes, Reviews in Mineralogy 16, Mineralogical Society of America, Washington, DC, 1986, pp. 185–225.
[4] B.E. Taylor, Degassing of Obsidian Dome rhyolite, Inyo volcanic chain, California, in: H.P. Taylor, Jr., J.R. O'Neil, J.R. Kaplan (Eds.), Stable Isotope Geochemistry: A Tribute to Samuel Epstein, Geochemical Society Special Publication 3, The Geochemical Society, San Antonio, TX, 1991, pp. 339–353.
[5] S.W. Anderson, J.H. Fink, Hydrogen isotope evidence for extrusion mechanisms of the Mount St. Helens lava dome, Nature 341 (1989) 521–523.
[6] J.C. Eichelberger, C.R. Carrigan, H.R. Westrich, R.H. Price, Non-explosive silicic volcanism, Nature 323 (1986) 598–602.
[7] J.H. Fink, S.W. Anderson, C.R. Manley, Textural constraints of effusive silicic magmatism: Beyond the permeable foam model, J. Geophys. Res. 97 (1992) 9073–9083.

[8] C. Jaupart, C.J. Allegre, Gas content, eruption rate and instabilities of eruption regime in silicic volcanoes, Earth Planet. Sci. Lett. 102 (1991) 413–429.
[9] J.H. Fink, S.W. Kieffer, Estimate of pyroclastic flow velocities resulting from explosive decompression of lava domes, Nature 363 (1993) 612–615.
[10] I. Friedman, R.L. Smith, W.D. Long, Hydration of natural glass and formation of perlite, Geol. Soc. Am. Bull. 77 (1966) 323–328.
[11] I. Friedman, J. Obradovich, Obsidian hydration dating of volcanic events, Quat. Res. (N. Y.) 16 (1981) 37–47.
[12] I. Friedman, F. Trembour, Obsidian hydration dating update, Am. Antiq. 48 (1983) 544–547.
[13] I. Friedman, Hydration rind dates rhyolite flows, Science 159 (1968) 878–880.
[14] I. Friedman, W.D. Long, J.D. Obradovich, Obsidian hydration dating, in: 9th Congress of the International Union for Quaternary Research, Abstracts, International Union for Quaternary Research 9, 1973, p. 105.
[15] I. Friedman, W. Long, Hydration rate of obsidian, Science 191 (1976) 347–352.
[16] Y. Zhang, E.M. Stolper, G.J. Wasserburg, Diffusion of a multi-species component and its role in oxygen and water transport in silicates, Earth Planet. Sci. Lett. 103 (1991) 228–240.
[17] N.W. Dunbar, P.R. Kyle, Volatile contents of obsidian clasts in tephra from the Taupo Volcanic Zone, New Zealand: Implications to eruptive processes, J. Volcanol. Geotherm. Res. 49 (1992) 127–145.
[18] C.G. MacPherson, D.R. Hilton, S. Newman, D.P. Mattey, CO_2, $^{13}C/^{12}C$ and H_2O variability in natural basaltic glasses: A study comparing stepped heating and FTIR spectroscopic techniques, Geochim. Cosmochim. Acta 63 (1999) 1805–1813.
[19] M. Sorey, U.S. Geological Survey, personal communication, 1996.
[20] P. Mariner, J.M. Donnelly-Nolan, U.S. Geological Survey, unpublished data, 1981.
[21] T.P. Rose, M.L. Davisson, R.E. Criss, Isotope hydrology of voluminous cold springs in fractured rock from an active volcanic region, northeastern California, J. Hydrol. 179 (1996) 207–236.
[22] P.D. Ihinger, Y. Zhang, E. Stolper, The speciation of dissolved water in rhyolitic melt, Geochim. Cosmochim. Acta 63 (1999) 3567–3578.
[23] C.W. Burnham, Development of the Burnham model for prediction of H_2O solubility in magmas, in: M.R. Carroll, J.R. Holloway (Eds.), Volatiles in Magmas, Reviews in Mineralogy 30, Mineralogical Society of America, Washington, DC, 1994, pp. 123–129.
[24] J.R. Holloway, J.G. Blank, Application of experimental results to C-O-H species in natural melts, in: M.R. Carroll, J.R. Holloway (Eds.), Volatiles in Magmas, Reviews in Mineralogy 30, Mineralogical Society of America, Washington, DC, 1994, pp. 187–230.
[25] J.H. Fink, R.W. Griffiths, Morphology, eruption rates, and rheology of lava domes: Insights from laboratory models, J. Geophys. Res. 103 (1998) 527–545.
[26] R.W. Griffiths, J.H. Fink, Solidifying Bingham extrusion: a model for growth of silicic lava domes, J. Fluid Mech. 347 (1997) 13–36.
[27] T.A. Vogel, L. Younker, B.C. Schuraytz, Constraints on magma ascent, emplacement, and eruption: Geochemical and mineralogical data from drill core samples at Obsidian Dome, Inyo Chain, CA, Geology 15 (1987) 405–408.
[28] D.A. Swanson, R.T. Holcomb, Regularities in growth of the Mount St. Helens dacite dome, 1980–1986, in: J.H. Fink (Ed.), Lava Flows and Domes, IAVCEI Proc. in Volcanol. 2, Springer-Verlag, New York, 1990, pp. 3–24.
[29] R.S.J. Sparks, Causes and consequences of pressurisation in lava dome eruptions, Earth Planet. Sci. Lett. 150 (1997) 177–189.
[30] O. Melnik, R.S.J. Sparks, Nonlinear dynamics of lava dome extrusion, Nature 402 (1999) 37–41.